

# Iodine oxide in the global marine boundary layer

C. Prados-Roman<sup>1</sup>, C. A. Cuevas<sup>1</sup>, T. Hay<sup>1</sup>, R. P. Fernandez<sup>1,\*</sup>, A. S. Mahajan<sup>1,\*\*</sup>,  
S-J. Royer<sup>2</sup>, M. Galí<sup>2,†</sup>, R. Simó<sup>2</sup>, J. Dachs<sup>3</sup>, K. Großmann<sup>4</sup>, D. E. Kinnison<sup>5</sup>, J-F.  
Lamarque<sup>5</sup> and A. Saiz-Lopez<sup>1</sup>

[1]{Atmospheric Chemistry and Climate Group, Institute of Physical Chemistry Rocasolano  
(CSIC), Madrid, Spain}.

[2]{Institute of Marine Sciences, (CSIC), Barcelona, Spain}.

[3]{Institute of Environmental Assessment and Water Research (CSIC), Barcelona, Spain}.

[4]{Institute of Environmental Physics, University of Heidelberg, Germany}.

[5]{Atmospheric Division, NCAR, Boulder, CO, USA}.

[\*]{now at: National Scientific and Technical Research Council (CONICET), UTN-FR  
Mendoza/ICB-UNCuyo, Mendoza, Argentina}.

[\*\*]{now at: Indian Institute of Tropical Meteorology, Pune, India}.

[†]{now at: Takuvik (UL/CNRS), Quebec, Canada}.

Correspondence to: a.saiz@csic.es.

## Abstract

Emitted mainly by the oceans, iodine is a halogen compound important for atmospheric chemistry due to its high ozone depletion potential and effect on the oxidizing capacity of the atmosphere. Here we present a comprehensive dataset of iodine oxide (IO) measurements in the open marine boundary layer (MBL) made during the Malaspina 2010 circumnavigation. Results show IO mixing ratios ranging from 0.4 to 1 pmol mol<sup>-1</sup> (30% uncertainty) and, complemented with additional field campaigns, this dataset confirms through observations the ubiquitous presence of reactive iodine chemistry in the global marine environment. We use a global model with organic (CH<sub>3</sub>I, CH<sub>2</sub>ICl, CH<sub>2</sub>I<sub>2</sub> and CH<sub>2</sub>IBr) and inorganic (HOI and I<sub>2</sub>)

1 iodine ocean emissions to investigate the contribution of the different iodine source gases to  
2 the budget of IO in the global MBL. In agreement with previous estimates, our results  
3 indicate that, globally averaged, the abiotic precursors contribute about 75% to the iodine  
4 oxide budget. However, this work reveals a strong geographical pattern in the contribution of  
5 organic vs. inorganic precursors to reactive iodine in the global MBL.

6

## 7 **1 Introduction**

8 The atmospheric relevance of reactive halogens became clear decades ago when their  
9 potential to catalytically destroy ozone ( $O_3$ ) was first recognised in the polar stratosphere  
10 (Molina and Rowland, 1974) and later on in the troposphere (e.g. Barrie et al., 1988).  
11 Halogens are also known to affect the  $NO_x$  ( $NO$ ,  $NO_2$ ) and  $HO_x$  ( $HO$ ,  $HO_2$ ) partitioning and  
12 the lifetime of organic compounds, to alter the sulphur and mercury cycles and, in the case of  
13 iodine oxides, to form ultra-fine particles in coastal areas (Saiz-Lopez and von Glasow, 2012  
14 and references therein).

15 Since the first study to deal with the tropospheric relevance of inorganic iodine (Chameides  
16 and Davis, 1980), major efforts have been made to detect reactive iodine species in their main  
17 source region: the oceans (Saiz-Lopez et al., 2012 and references therein). Several field  
18 campaigns in scattered marine environments have aimed at detecting iodine oxide - beacon  
19 for the presence of active iodine chemistry- and determining the nature and strength of  
20 organic and inorganic source gases of iodine (referenced hereafter as OSG, ISG, respectively).  
21 Air-sea fluxes of iodocarbons ( $CH_3I$ ,  $CH_2I_2$ ,  $CH_2ICl$  and  $CH_2IBr$ ,  $C_2H_5I$ , 1- $C_3H_7I$ , 2- $C_2H_7I$ )  
22 have been reported (Carpenter et al., 2012), but in general observations were insufficient to  
23 explain measured IO concentrations in the MBL, implying the existence of an abiotic ocean  
24 source of iodine (Mahajan et al., 2010; Jones et al., 2010; Mahajan et al., 2012; Gómez Martín  
25 et al., 2013a; Großmann et al., 2013; Lawler et al., 2014). In several one-dimensional model  
26 studies simulated emissions of molecular iodine ( $I_2$ ) were used to fit IO observations (e.g.  
27 Mahajan et al., 2010; Großmann et al., 2013), however the recent work of Lawler et al. (2014)  
28 with the first observation of  $I_2$  in the remote MBL, confirmed that the emission of  $I_2$  is still  
29 insufficient to explain the observed levels of IO. Recently, the study of Carpenter et al. (2013)  
30 has experimentally confirmed that not only  $I_2$  is emitted naturally from the oceans but also,  
31 and mainly, hypoiodous acid (HOI). In that study and in the subsequent work of MacDonald  
32 et al. (2014), the authors have confirmed through laboratory work that the oceanic emission of

1 ISG (HOI and I<sub>2</sub>) follows the deposition of tropospheric O<sub>3</sub> to the oceans and its reaction with  
2 aqueous iodide (I<sub>aq</sub><sup>-</sup>, Garland et al., 1980), and they proposed a parameterisation for ocean  
3 ISG emissions dependent on O<sub>3</sub>, wind speed (ws) and sea surface temperature (SST).

4 In this work, we present a comprehensive map of IO observations in the global MBL showing  
5 the ubiquity of this radical in the marine environment. Moreover, by means of a global model  
6 including OSG and ISG oceanic emissions; we investigate the geographical emission patterns  
7 of both iodine precursors and their contribution to the IO budget in the marine environment.  
8 Section 2 details the measurement campaign of Malaspina 2010 and provides information on  
9 the chemical model used throughout this work. Section 3 presents the results of the IO  
10 observations and the modelling studies, and Section 4 concludes this work.

11

## 12 **2 Measurements and model**

13 In the following we present the setup of the O<sub>3</sub> and IO measurements during the Malaspina  
14 2010 expedition as well as the model schemes used in this study.

### 15 **2.1 Measurements during the Malaspina 2010 circumnavigation**

16 From December 2010 until July 2011 the Spanish research vessel Hesperides  
17 circumnavigated the World's oceans within the framework of the Malaspina 2010 project.  
18 The main objectives of this interdisciplinary campaign were to investigate the  
19 biogeochemistry, physical properties and microbiological biodiversity of the oceans; the  
20 genetic diversity of the deep-ocean and the exchange of trace gases and pollutants with the  
21 atmosphere; and assessing the impact of global change in the ocean. The different legs of the  
22 cruise and the docking dates are indicated in Table 1.

23 A Multi-Axis Differential Optical Absorption Spectroscopy instrument (MAX-DOAS; Platt  
24 and Stutz, 2008) and a commercial 2B-205 ozone monitor, along with a GPS, were deployed  
25 aboard the vessel in order to investigate the presence of atmospheric trace gases such as IO,  
26 O<sub>3</sub>, BrO, HCHO and CHOCHO in the MBL. Herein we focus on the observations of IO and  
27 O<sub>3</sub> during the campaign.

### 1 **2.1.1 Surface ozone**

2 The ozone monitor was installed in the ship's bridge with a 5 m long Teflon-lined inlet tube  
3 from the upper deck, well forward of the exhaust stacks (~15 m above sea level (m.a.s.l.)).  
4 The inlet was placed just above the railing in the air coming from the front of the ship,  
5 avoiding sampling air from the ship's boundary layer. Due to GPS communication errors, our  
6 data compilation started on 21/02/2011 (2<sup>nd</sup> leg) and finished on 12/07/2011.

7 The ozone volume mixing ratios (vmr) observed during Malaspina 2010 are presented in Fig.  
8 1a along with the ancillary measurements of relevance for the present work (i.e., SST and ws;  
9 Fig. 1 and Table 2). Simulations of the 5-day backward trajectories of the air masses arriving  
10 at the ship's track are provided in Fig. 2, showing the typical non-continental origin of the air  
11 masses sensed during the cruise.

### 12 **2.1.2 Iodine oxide**

13 Aiming at the detection of IO along the Malaspina's track, a MAX-DOAS instrument was  
14 installed on the second deck near the rear of the ship (~10 m.a.s.l.). Briefly, these instruments  
15 measure the intensity of scattered light in the UV-VIS range entering a scanning telescope at  
16 several precise viewing angles and have been widely used for atmospheric composition  
17 research (Platt and Stutz, 2008). Thus only a summary of the particular MAX-DOAS  
18 instrument mounted on the Hesperides research vessel is given hereafter. For details regarding  
19 the MAX-DOAS technique please refer to the work of, e.g., Platt and Stutz (2008) and  
20 Hönninger et al. (2004) and for further details of our ship-based MAX-DOAS instrument  
21 please see Mahajan et al. (2012).

22 Briefly, in the case of the Malaspina's MAX-DOAS instrument, the scanning telescope was  
23 housed in a weatherproof metal chamber with a flat UV-transmitting acrylic window, with a  
24 sunshade to reduce spectral effects on the window. The telescope unit (built by the New  
25 Zealander National Institute of Water and Atmospheric Research-NIWA) was mounted on a  
26 gimbal table to compensate for the pitch and roll of the ship. The gimbal dampened the  
27 effective oscillations in telescope elevation angle to  $\pm 1^\circ$  for most of the cruise and  $\pm 2^\circ$  in  
28 rough conditions. In addition, a high accuracy ( $\pm 0.1^\circ$ ), fast response (0.3 s) inclinometer was  
29 used to log the residual oscillations in order to correct the elevation angles. Only true angles  
30 within  $0.2^\circ$  of each prescribed elevation angle were used for analysis. The azimuth viewing  
31 direction was towards the ship's bow ( $20^\circ$  anticlockwise) to minimize exhaust emissions in the

1 line of sight. The scanning telescope consisted of a rotating diagonal mirror driven by a  
2 stepper motor and a 50.8 mm diameter fused silica lens with a focal length of 200 mm, giving  
3 a field of view of 0.5°. The light was focused onto a 5 m long 19 optic fibre bundle leading to  
4 a Princeton Instruments SP500i spectrometer with a Princeton Instruments Pixis 400B CCD  
5 camera. A 600 grooves mm<sup>-1</sup> grating was used, giving approximately an 80 nm spectral  
6 window and a spectral resolution of 0.5 nm FWHM. Spectra were recorded for a short  
7 exposure time of 1 s at each discrete elevation angle (2, 4, 6, 8, 10, 15, 30 and 90°) in order to  
8 minimize potential deviations in angle due to the ship's movement. The scan sequence was  
9 repeated every 2 min and after every 10 cycles the grating was shifted between the two  
10 wavelength regions, centred on 358 nm (UV spectral range) and 440 nm (VIS spectral range).  
11 Results presented in this work correspond to the VIS channel, where IO could be measured  
12 (see Sect. 3.1).

## 13 **2.2 Modelling the oceanic emissions of reactive iodine precursors**

14 We implemented the experimentally derived ocean fluxes of ISG (Carpenter et al., 2013;  
15 MacDonald et al., 2014) into the global chemistry-climate model CAM-Chem (Community  
16 Atmospheric Model with Chemistry, version 4.0; Lamarque et al., 2012), which already  
17 included a validated OSG emissions inventory and a state-of-the-art halogen chemistry  
18 scheme (Ordóñez et al., 2012). The on-line ISG flux formulation, based on the studies of  
19 Carpenter et al. (2013) and MacDonald et al. (2014), was performed considering the  
20 instantaneous modelled levels of surface O<sub>3</sub>, SST and ws in each of the model grid-boxes over  
21 the oceans (i.e., imposing an ocean mask). In the following we summarise the model schemes  
22 used in this work. Further details on the particular implementation of the ISG  
23 parameterisation into the CAM-Chem model are given in Prados-Roman et al. (2014),  
24 whereas the general model setup is described in the study of Lamarque et al. (2012).

### 25 **2.2.1 Model schemes**

26 Throughout this work, two different pairs of simulations were performed in order to evaluate  
27 the model, to identify the contribution of OSG/ISG fluxes and to estimate the iodine burden of  
28 the MBL. A brief description of the simulations used in this study is given below.

29 (1) *Base-Organic runs*. In the *Base run*, simulations were performed considering the  
30 oceanic emission of organic and inorganic iodine precursors. Based on previous  
31 publications, the OSG inventory of very-short lived iodocarbons (OSG= CH<sub>3</sub>I,

1 CH<sub>2</sub>I<sub>2</sub>, CH<sub>2</sub>I<sub>2</sub>Br and CH<sub>2</sub>I<sub>2</sub>Cl) was considered (Ordóñez et al., 2012), while the ISG  
2 computation of HOI and I<sub>2</sub> was used as described in the study of Prados-Roman et  
3 al., 2014. In order to distinguish the contribution of the inorganic and the organic  
4 iodine source gases to the IO budget in the MBL, the *Organic* scheme included only  
5 the abovementioned OSG (by forcing the inorganic emissions to be null). Hence, the  
6 contribution of ISG to the IO budget in the MBL (i.e., IO<sub>ISG</sub>) was defined as the  
7 difference between the IO vmr obtained in the MBL after the *Base run*  
8 (IO=IO<sub>ISG</sub>+OSG), and the IO vmr obtained after the *Organic run* (i.e., IO<sub>OSG</sub>). That is  
9 IO<sub>ISG</sub>= (IO) - (IO<sub>OSG</sub>); and the relative contribution of ISG to IO was defined as  
10 (IO<sub>ISG</sub>)/(IO) in percentage. Similarly, the contribution of each individual iodocarbon  
11 to the budget of IO was investigated.

12 (2) *NoPhot-Phot runs*. It is known that the self-reaction of IO in pristine conditions  
13 yields the formation of higher oxides (I<sub>2</sub>O<sub>x</sub>, x=2, 3 or 4). However, once formed, the  
14 reaction pathways of these compounds are still not well understood. One possibility  
15 is their nucleation into ultra-fine particles as observed in coastal areas (Gómez  
16 Martín et al., 2013b). Those conditions were however not representative of the  
17 Malaspina expedition since most of the marine atmosphere crossed was  
18 representative of open ocean environment. A possible pathway for Malaspina's  
19 conditions was the photodissociation of those I<sub>2</sub>O<sub>x</sub> into OIO+I, OIO+IO or OIO+OIO  
20 as previously modelled for the Antarctic (Saiz-Lopez et al., 2008) and global marine  
21 troposphere (Saiz-Lopez et al., 2014), which would therefore result in additional  
22 reactive iodine in the MBL. The so-called *Phot run* included I<sub>2</sub>O<sub>x</sub> photolysis while  
23 the simulation excluding such photolysis was referred to as *NoPhot run*. Note that,  
24 unless stated otherwise, in the aforementioned *Base-Organic* schemes the I<sub>2</sub>O<sub>x</sub> were  
25 not allowed to photolyse but, once formed, they were lost by thermal decomposition  
26 or to pre-existing aerosols instead.

27 All simulations were performed with a horizontal grid resolution of 1.9° (latitude) × 2.5°  
28 (longitude) and 26 hybrid vertical levels (0-40 km), and considered the SST and sea-ice  
29 boundary conditions representative of year 2000 (Rayner et al., 2003). Note that, since the  
30 model was not run with specified dynamics, simulations are not representative of the  
31 meteorology of any specific year. Thus, unless stated the opposite, the model results presented  
32 in this work correspond to 24 h annual averages.

33

### 1   **3 Results and discussions**

2   In this section we present the observations of IO in the MBL and compare them to different  
3   model runs. Furthermore, we investigate the contribution of the OSG and ISG fluxes to the IO  
4   budget in the MBL.

#### 5   **3.1 Observations of IO in the global marine boundary layer**

6   During Malaspina 2010 IO was detected above instrumental detection limit ( $1.2\text{-}3.5 \times 10^{13}$   
7   molec cm<sup>-2</sup>) in all marine environments sampled. Figure 3 shows a typical IO spectral fit  
8   during that expedition and the IO differential slant column densities (dSCD) measured along  
9   the cruise track. Note that diverse filters were used in this dataset for quality assurance (e.g.,  
10   cloud and wind direction filters). Following previous studies and using only IO dSCD above  
11   the quality filters, the IO mixing ratios were inferred by the well-established "O<sub>4</sub> method"  
12   (Wagner et al., 2004), after validating results of several days with a radiative transfer model  
13   (RTM) (e.g., Mahajan et al., 2012; Gómez Martín et al., 2013a). Particular details on these  
14   procedures (IO spectral and vmr retrieval) as well as the quality filters applied are provided in  
15   the Supplementary Information (SI).

16   Overall, during the Malaspina expedition the IO radical was constantly observed in the  
17   daytime MBL over three oceans and both hemispheres. The IO vmr integrated in the MBL  
18   ranged between 0.4 and 1 pmol mol<sup>-1</sup> (detection limit of  $\sim 0.2$  pmol mol<sup>-1</sup>), with lower values  
19   measured over the South Atlantic waters and with the highest levels in the marine region west  
20   of Mexico. Figure 4 shows the averaged daytime IO vmr of the Malaspina dataset, along with  
21   IO vmr obtained from former field campaigns: Cape Verde (Read et al., 2008; Mahajan et al.,  
22   2010), HaloCAST-P (Mahajan et al., 2012), CHARLEX (Gómez Martín et al., 2013a) and  
23   TransBrom (Großmann et al., 2013); and also the value measured in the MBL by Dix et al.  
24   (2013) during a research flight. Note that the IO vmr reported for each of these campaigns are  
25   by definition intrinsically linked to the specific viewing geometry of each DOAS instrument  
26   (Platt and Stutz, 2008). During the Cape Verde campaign a Long Path-DOAS instrument was  
27   used with a fixed light path at 10 m.a.s.l. (Read et al., 2008; Mahajan et al., 2010). In all the  
28   other campaigns shown in Fig. 4, MAX-DOAS instruments were employed. Given the  
29   different viewing elevation angles and instrumental setup, each of those MAX-DOAS  
30   instruments sensed a different part of the MBL (Platt and Stutz, 2008; Hönninger et al., 2004;  
31   Wagner et al., 2004). Although sensitivity RTM studies performed during each of those

1 MAX-DOAS campaigns agreed on a decreasing vertical profile of IO in the MBL, the  
2 generally poor information content of the measurements hindered the vertical resolution of the  
3 inferred IO vmr vertical profiles and the reported vmr were therefore linked to a given sensed  
4 layer; particularly 0-200 m during HaloCAST-P and TransBrom (Mahajan et al., 2012;  
5 Großmann et al., 2013), 0-1200 m during CHARLEX (Gómez Martín et al., 2013a), 0-800 m  
6 during the research flight (Dix et al, 2013) and 0-600 m during Malaspina (this work, SI).  
7 Therefore the values reported in Fig. 4 should be considered as the mean IO vmr in each of  
8 the aforementioned altitude ranges linked to a given elevation angle (e.g., 2° in the case of  
9 Malaspina). Note that, despite these unavoidable retrieval limitations, Fig. 4 proofs the  
10 ubiquity of IO in the global MBL and hence the presence of reactive iodine chemistry in all  
11 sub-polar marine environments.

### 12 **3.2 Observations vs. model**

13 Figure 4 shows the most comprehensive map of IO observations in the remote marine  
14 environment. We now use these observations together with the CAM-Chem model to evaluate  
15 the geographical distribution of IO in the MBL. The performance of the model was evaluated  
16 by comparing modelled and observed IO mixing ratios in the MBL for the aforementioned  
17 particular altitude range sensed during each campaign. Note that, as mentioned above, a key  
18 parameter in the model setup is the flux of ISG, which depends mainly on O<sub>3</sub> and ws  
19 (Carpenter et al., 213; MacDonald et al., 2014). Hence, even though Fig. 4 shows IO  
20 measurements from 6 different field campaigns, surface O<sub>3</sub>, ws and IO were not measured  
21 simultaneously in all of them. Thus, only the campaigns of Malaspina, CHARLEX and Cape  
22 Verde were chosen for comparison with the model. Figure 5 presents this comparison  
23 exercise, where the IO vmr observations in three oceans and both hemispheres are juxtaposed  
24 to the model output after the *Organic* scheme and after the *Base* run considering the *NoPhot*  
25 and the *Phot* schemes. For this exercise the model was sampled at the same time (month) of  
26 the year and geolocation as the measurements (considering the model grid resolution of 1.9°  
27 latitude x 2.5° longitude). Note that the low IO vmr resulting after the *Organic* run remains  
28 basically unaltered despite the photolysis scheme considered. Thus for simplicity only the  
29 *Organic-NoPhot* output (i.e., *Organic* run) is shown in Fig. 5.  
30 Considering the ISG emissions, along with OSG, the model reproduces satisfactorily the IO  
31 observations (Fig. 5). Note that, as found in the *Organic* run, the emission of OSG alone  
32 explains on average only ~25% of the IO levels observed over the different oceans,



1 percentage that agrees well with previous one-dimensional model studies performed at  
2 specific marine environments (Mahajan et al., 2010; Jones et al., 2010; Mahajan et al., 2012;  
3 Gómez Martín et al., 2013a; Großmann et al., 2013; Lawler et al., 2014). This result points out  
4 the importance of including ISG emissions in global models. Regarding the *Base* run results,  
5 in general the *NoPhot* run reproduces the observations although in some regions the *Phot*  
6 scheme is closer to the measurements (Fig. 5). Note that the modelled IO vmr in the *Phot*  
7 scheme- likely to be a more realistic scheme for  $I_2O_x$  (Saiz-Lopez et al., 2014)- can even  
8 double the IO vmr given by the *NoPhot* scheme, stressing the need of further efforts from the  
9 community to investigate the fate of these higher iodine oxides. However, since the photolysis  
10 rates of  $I_2O_x$  are currently subject to uncertainty (Saiz-Lopez et al., 2014), hereafter only the  
11 *NoPhot* scheme is considered bearing, thus, the results presented as lower limits.

12

### 13 **3.3 Sources of IO in the global marine boundary layer**

14 After analysing the consistency of modelled vs. measured IO, in this section we investigate  
15 the sensitivity of the IO levels towards the different modelled iodine precursors. Considering  
16 the OSG emission inventory (Ordóñez et al., 2012) and the ISG (Prados-Roman et al., 2014),  
17 the modelled OSG/ISG ratio allows quantifying the individual sources and total oceanic  
18 emissions of iodine to the atmosphere. Results indicate that, globally averaged, the total  
19 oceanic iodine emissions yield  $2.3 \text{ Tg y}^{-1}$ . From these, only 17% ( $0.4 \text{ Tg y}^{-1}$ ) originate from  
20 organic sources, which are related to bacteria, microalgae, phytoplankton, etc. (Carpenter et  
21 al., 2012). On a global average, nearly half (43%) of the organic flux derives from  $CH_3I$ , 29%  
22 from  $CH_2ICl$ , 19% from  $CH_2I_2$  and 9% from  $CH_2IBr$ , although their temporal and spatial  
23 distribution varies with, e.g., the solar radiation at sea surface and the properties of the ocean  
24 mixed layer (Bell et al., 2002; Carpenter et al., 2012; Ordóñez et al., 2012). The sea-air  
25 exchange of iodine is thus driven mainly by abiotic sources. Our results indicate that, globally  
26 averaged,  $1.9 \text{ Tg (I) y}^{-1}$  (i.e., 83% of the total oceanic iodine fluxes) are emitted to the MBL  
27 as a result of the reaction of tropospheric  $O_3$  with  $I_{aq}^-$  in the ocean surface; and that the  
28 partitioning of these ISG emissions is directed by HOI (95% HOI, 5%  $I_2$ ; Prados-Roman et  
29 al., 2014).

30 Figure 6a provides the annually averaged burden of IO in the global MBL, with values  
31 ranging from less than  $0.05 \text{ pmol mol}^{-1}$  in the sub-polar waters; to  $\sim 0.9 \text{ pmol mol}^{-1}$  above  
32 waters offshore the Baja California peninsula. Figure 6b shows the geographical pattern of the

1 contribution of ISG to the IO budget (i.e.,  $IO_{ISG}$ ). The model results indicate that, globally  
2 averaged, about 75% of the IO in the MBL derives from inorganic precursors. As mentioned  
3 in the previous section, as an averaged value, this result is indeed consistent with previous  
4 estimates at given transects along the Pacific Ocean or offshore waters of Cape Verde and  
5 Galapagos Islands (Mahajan et al., 2010; Jones et al., 2010; Mahajan et al., 2012; Gómez  
6 Martín et al., 2013a; Großmann et al., 2013; Lawler et al., 2014). However, our model results  
7 show the uneven geographical distribution of  $IO_{ISG}$ , e.g., marine tropical regions in the  
8 southern hemisphere where  $IO_{ISG}$  is of 40%; or regions of ozone-related pollution outflow  
9 such the Bay of Bengal or the Gulf of Mexico (Myhre et al., 2013, see also SI) where, as a  
10 consequence of the  $O_3-I_{aq}^-$  interaction,  $IO_{ISG}$  can be more than 90%. Figure 7 shows the  
11 contribution of each of the four modelled iodocarbons to IO in the MBL, indicating that in the  
12 biological active regions of the tropics IO derives mainly from the dihalomethanes ( $CH_2ICl >$   
13  $CH_2I_2 > CH_2IBr$ ) and to a lesser extend to  $CH_3I$ . Out of those regions  $CH_3I$  dominates the  
14 organic contribution to IO in the MBL, increasing with latitude as a result of its longer  
15 lifetime (Bell et al., 2002). Note however that the model simulations presented here do not  
16 include iodine emissions, organic or inorganic, from ice surfaces. Also, the strong dependence  
17 of the ISG flux with SST considerably reduces the inorganic iodine emissions over the cold  
18 waters in the high latitudes. Furthermore, as detailed in the study of MacDonald et al. (2014),  
19 the uncertainty on the parameterisation of ISG increases with decreasing SST. Thus, in the  
20 polar marine regions our simulated inorganic contribution to the IO budget should be  
21 regarded with caution. Despite these uncertainties, overall the main source of IO in the MBL  
22 at a global scale is HOI. However, as shown in Fig. 6b and Fig. 7, this is subject to strong  
23 spatial patterns in emission with regions in the southern hemisphere where the OSG can  
24 account for up to 50% of the modelled IO levels.

25

## 26 **4 Summary**

27 Here we present a comprehensive set of observations of iodine oxide mixing ratios in the  
28 marine boundary layer obtained after the Malaspina 2010 circumnavigation covering three  
29 non-polar oceans and both hemispheres. Complementing this dataset with measurements  
30 gained after campaigns in the tropical Atlantic Ocean and in the Eastern and Western Pacific  
31 Ocean, we provide field evidence for the ubiquitous presence of IO, and thus reactive iodine  
32 chemistry, in the global marine environment. By comparing these measurements with model

1 results, we confirm the need of including the inorganic oceanic emissions of iodine into  
2 global models, and also stress the need for further laboratory and theoretical studies about the  
3 atmospheric fate of  $I_2O_x$ . In particular, the model results indicate that 83% of the total oceanic  
4 natural emissions of iodine are inorganic (mainly HOI) following the reaction of iodide with  
5 ozone at the sea surface; and these inorganic emissions are indeed necessary to reproduce the  
6 observations of IO in all marine environments. Finally, our results show that the contribution  
7 of the organic/inorganic source gases to IO levels in the global MBL is geographically highly  
8 variable, existing regions of ozone-rich outflow where the inorganic contribution to IO can be  
9 more than 90%. This combined observational and modelling exercise strengthens the need of  
10 including both the organic and the inorganic oceanic emissions of iodine into global models  
11 for a more accurate assessment of the oxidizing capacity of the marine troposphere.

12

### 13 **Acknowledgements**

14 The authors would like to thank everyone involved in the Malaspina 2010 expedition, funded  
15 by the Spanish Ministry of Economy and Competitiveness. In particular the Marine  
16 Technology Unit (UTM-CSIC) for facilitating the ancillary data as well as the Hesperides  
17 R/V crew. We also thank Alan Thomas, John Robinson and Dave Humphries (NIWA) for  
18 building the MAX-DOAS tracker and the atmospheric group of the Institute of Environmental  
19 Physics (Heidelberg) for facilitating the gimbal table. We also thank Markus Rex for his  
20 comments on the ozone measurements during the TransBrom campaign, and Klaus  
21 Pfeilsticker and John Plane for helpful discussions. The Indian Institute of Tropical  
22 Meteorology is supported by the Ministry of Earth Sciences, Government of India. R.P.F  
23 would like to thank ANPCyT (PICT-PRH 2009-0063) for financial support. The data  
24 supporting this article can be requested from the corresponding author A.S-L (a.saiz@csic.es).

25

26

### 27 **References**

28 Barrie, L. A., Bottenheim, J. W., Schnell, R. C., Crutzen, P. J., and Rasmussen, R. A.: Ozone  
29 depletion and photochemical reactions at polar sunrise in the lower Arctic atmosphere,  
30 Nature, 334, 138-141, 1988.

1 Bell, N., Hsu, L., Jacob, D. J., Schultz, M. G., Blake, D. R., Butler, J. H., King, D. B., Lobert,  
2 J. M., and Maier-Reimer, E.: Methyl iodide: Atmospheric budget and use as a tracer of marine  
3 convection in global models, *Journal of Geophysical Research: Atmospheres*, 107, 4340,  
4 10.1029/2001JD001151, 2002.

5 Carpenter, L. J., Archer, S. D., and Beale, R.: Ocean-atmosphere trace gas exchange, *Chem.*  
6 *Soc. Rev.*, 41, 6473-6506, 10.1039/C2CS35121H, 2012.

7 Carpenter, L. J., MacDonald, S. M., Shaw, M. D., Kumar, R., Saunders, R. W., Parthipan, R.,  
8 Wilson, J., and Plane, J. M. C.: Atmospheric iodine levels influenced by sea surface emissions  
9 of inorganic iodine, *Nature Geosci.*, 6, 108-111, 2013.

10 Chameides, W. L., and Davis, D. D.: Iodine: Its possible role in tropospheric photochemistry,  
11 *J. Geophys. Res.*, 85, 7383-7398, 1980.

12 Dix, B., Baidar, S., Bresch, J. F., Hall, S. R., Schmidt, K. S., Wang, S., and Volkamer, R.:  
13 Detection of iodine monoxide in the tropical free troposphere, *Proceedings of the National*  
14 *Academy of Sciences*, 110, 2035-2040, 2013.

15 Draxler, R.R. and Rolph, G.D.: HYSPLIT (HYbrid Single-Particle Lagrangian Integrated  
16 Trajectory) Model access via NOAA ARL READY Website  
17 (<http://ready.arl.noaa.gov/HYSPLIT.php>). NOAA Air Resources Laboratory, Silver Spring,  
18 MD, 2014.

19 Garland, J. A., Elzerman, A. W., and Penkett, S. A.: The Mechanism for Dry Deposition of  
20 Ozone to Seawater Surfaces, *J. Geophys. Res.*, 85, 7488-7492, 1980.

21 Gómez Martín, J. C., Mahajan, A. S., Hay, T. D., Prados-Román, C., Ordóñez, C.,  
22 MacDonald, S. M., Plane, J. M. C., Sorribas, M., Gil, M., Paredes Mora, J. F., Agama Reyes,  
23 M. V., Oram, D. E., Leedham, E., and Saiz-Lopez, A.: Iodine chemistry in the eastern Pacific  
24 marine boundary layer, *Journal of Geophysical Research: Atmospheres*, 118, 887-904,  
25 10.1002/jgrd.50132, 2013a.

26 Gómez Martín, J. C., Gálvez, O., Baeza-Romero, M. T., Ingham, T., Plane, J. M. C., and  
27 Blitz, M. A.: On the mechanism of iodine oxide particle formation, *Phys. Chem. Chem. Phys.*,  
28 15, 15612-15622, 10.1039/C3CP51217G, 2013b.

29 Großmann, K., Frieß, U., Peters, E., Wittrock, F., Lampel, J., Yilmaz, S., Tschritter, J.,  
30 Sommariva, R., von Glasow, R., Quack, B., Krüger, K., Pfeilsticker, K., and Platt, U.: Iodine

1 monoxide in the Western Pacific marine boundary layer, *Atmos. Chem. Phys.*, 13, 3363-3378,  
2 10.5194/acp-13-3363-2013, 2013.

3 Hönniger, G., Friedeburg, C. v., and Platt, U.: Multi axis differential optical absorption  
4 spectroscopy (MAX-DOAS), *Atmos. Chem. Phys.*, 4, 231-254, 2004.

5 Jones, A. E., Anderson, P. S., Wolff, E. W., Roscoe, H. K., Marshall, G. J., Richter, A.,  
6 Brough, N., and Colwell, S. R.: Vertical structure of Antarctic tropospheric ozone depletion  
7 events: characteristics and broader implications, *Atmos. Chem. Phys.*, 10, 7775-7794,  
8 10.5194/acp-10-7775-2010, 2010.

9 Lamarque, J. F., Emmons, L. K., Hess, P. G., Kinnison, D. E., Tilmes, S., Vitt, F., Heald, C.  
10 L., Holland, E. A., Lauritzen, P. H., Neu, J., Orlando, J. J., Rasch, P. J., and Tyndall, G. K.:  
11 CAM-chem: description and evaluation of interactive atmospheric chemistry in the  
12 Community Earth System Model, *Geosci. Model Dev.*, 5, 369-411, 10.5194/gmd-5-369-2012,  
13 2012.

14 Lawler, M. J., Mahajan, A. S., Saiz-Lopez, A., and Saltzman, E. S.: Observations of I<sub>2</sub> at a  
15 remote marine site, *Atmos. Chem. Phys.*, 14, 2669-2678, 10.5194/acp-14-2669-2014, 2014.

16 MacDonald, S. M., Gómez Martín, J. C., Chance, R., Warriner, S., Saiz-Lopez, A., Carpenter,  
17 L. J., and Plane, J. M. C.: A laboratory characterisation of inorganic iodine emissions from the  
18 sea surface: dependence on oceanic variables and parameterisation for global modelling,  
19 *Atmos. Chem. Phys.*, 14, 5841-5852, 10.5194/acp-14-5841-2014, 2014.

20 Mahajan, A. S., Plane, J. M. C., Oetjen, H., Mendes, L., Saunders, R. W., Saiz-Lopez, A.,  
21 Jones, C. E., Carpenter, L. J., and McFiggans, G. B.: Measurement and modelling of  
22 tropospheric reactive halogen species over the tropical Atlantic Ocean, *Atmos. Chem. Phys.*,  
23 10, 4611-4624, 10.5194/acp-10-4611-2010, 2010.

24 Mahajan, A. S., Gómez Martín, J. C., Hay, T. D., Royer, S. J., Yvon-Lewis, S., Liu, Y., Hu,  
25 L., Prados-Roman, C., Ordóñez, C., Plane, J. M. C., and Saiz-Lopez, A.: Latitudinal  
26 distribution of reactive iodine in the Eastern Pacific and its link to open ocean sources,  
27 *Atmos. Chem. Phys.*, 12, 11609-11617, 10.5194/acp-12-11609-2012, 2012.

28 Mahajan, A. S., Prados-Roman, C., Hay, T. D., Lampel, J., Pöhler, D., Großmann, K.,  
29 Tschritter, J., Frieß, U., Platt, U., Johnston, P., Kreher, K., Wittrock, F., Burrows, J. P., Plane,  
30 J. M. C., and Saiz-Lopez, A.: Glyoxal observations in the global marine boundary layer,

1 Journal of Geophysical Research: Atmospheres, 119, 2013JD021388,  
2 10.1002/2013JD021388, 2014.

3 Molina, M. J., and Rowland, F. S.: Stratospheric sink for chlorofluoromethanes: Chlorine-  
4 atom catalysed destruction of ozone, *Nature*, 249, 810-812, 1974.

5 Myhre, G., D. Shindell, D., Bréon, F.-M., Collins, W., Fuglestedt, J., Huang, J., Koch, D.,  
6 Lamarque, J.-F., Lee, D., Mendoza, B., Nakajima, T., Robock, A., Stephens, G., Takemura, T.  
7 and Zhang, H.: Anthropogenic and Natural Radiative Forcing. In: *Climate Change 2013: The*  
8 *Physical Science Basis. Contribution of Working Group I to the Fifth Assessment Report of*  
9 *the Intergovernmental Panel on Climate Change* [Stocker, T.F., D. Qin, G.-K. Plattner, M.  
10 Tignor, S.K. Allen, J. Boschung, A. Nauels, Y. Xia, V. Bex and P.M. Midgley (eds.)].  
11 Cambridge University Press, Cambridge, United Kingdom and New York, NY, USA, Chap.  
12 8, 2013.

13 Ordóñez, C., Lamarque, J. F., Tilmes, S., Kinnison, D. E., Atlas, E. L., Blake, D. R., Sousa  
14 Santos, G., Brasseur, G., and Saiz-Lopez, A.: Bromine and iodine chemistry in a global  
15 chemistry-climate model: description and evaluation of very short-lived oceanic sources,  
16 *Atmos. Chem. Phys.*, 12, 1423-1447, 10.5194/acp-12-1423-2012, 2012.

17 Platt, U., and Stutz, J.: Differential Absorption Spectroscopy, in: *Differential Optical*  
18 *Absorption Spectroscopy, Physics of Earth and Space Environments*, Springer, Berlin  
19 Heidelberg, 135-174, 2008.

20 Prados-Roman, C., Cuevas, C., Fernandez, R. P., Kinnison, D. E., Lamarque, J.-F., and Saiz-  
21 Lopez, A.: A negative feedback between anthropogenic ozone pollution and enhanced ocean  
22 emissions of iodine, accepted for ACPD, 2014.

23 Rayner, N. A., Parker, D. E., Horton, E. B., Folland, C. K., Alexander, L. V., Rowell, D. P.,  
24 Kent, E. C., and Kaplan, A.: Global analyses of sea surface temperature, sea ice, and night  
25 marine air temperature since the late nineteenth century, *Journal of Geophysical Research:*  
26 *Atmospheres*, 108, 4407, 10.1029/2002JD002670, 2003.

27 Read, K. A., Mahajan, A. S., Carpenter, L. J., Evans, M. J., Faria, B. V. E., Heard, D. E.,  
28 Hopkins, J. R., Lee, J. D., Moller, S. J., Lewis, A. C., Mendes, L., McQuaid, J. B., Oetjen, H.,  
29 Saiz-Lopez, A., Pilling, M. J., and Plane, J. M. C.: Extensive halogen-mediated ozone  
30 destruction over the tropical Atlantic Ocean, *Nature*, 453, 1232-1235, 2008.

1 Saiz-Lopez, A., Plane, J. M. C., Mahajan, A. S., Anderson, P. S., Bauguitte, S. J.-B., Jones, A.  
2 E., Roscoe, H. K., Salmon, R. A., Bloss, W. J., Lee, J. D., and Heard, D. E.: On the vertical  
3 distribution of boundary layer halogens over coastal Antarctica: implications for O<sub>3</sub>, HO<sub>x</sub>,  
4 NO<sub>x</sub> and the Hg lifetime, *Atmos. Chem. Phys.*, 8, 887-900, 2008.

5 Saiz-Lopez, A., and von Glasow, R.: Reactive halogen chemistry in the troposphere, *Chem.*  
6 *Soc. Rev.*, 41, 6448-6472, 10.1039/C2CS35208G, 2012.

7 Saiz-Lopez, A., Plane, J. M. C., Baker, A. R., Carpenter, L. J., Von Glasow, R., Gómez  
8 Martín, J. C., McFiggans, G., and Saunders, R. W.: Atmospheric Chemistry of Iodine, *Chem.*  
9 *Rev. (Washington, DC, U. S.)*, 112, 1773-1804, 10.1021/cr200029u, 2012.

10 Saiz-Lopez, A., Fernandez, R. P., Ordóñez, C., Kinnison, D. E., Gómez Martín, J. C.,  
11 Lamarque, J. F., and Tilmes, S.: Iodine chemistry in the troposphere and its effect on ozone,  
12 *Atmos. Chem. Phys. Discuss.*, 14, 19985-20044, 10.5194/acpd-14-19985-2014, 2014.

13 Wagner, T., Dix, B., Friedeburg, C. v., Frieß, U., Sanghavi, S., Sinreich, R., and Platt, U.:  
14 MAX-DOAS O<sub>4</sub> measurements: A new technique to derive information on atmospheric  
15 aerosols—Principles and information content, *Journal of Geophysical Research:*  
16 *Atmospheres*, 109, D22205, 10.1029/2004JD004904, 2004.

17

1 Table 1. Description of the different legs of the Malaspina 2010 expedition. Due to technical  
 2 problems, the O<sub>3</sub> and IO measurements presented in this work correspond to the period from  
 3 21/02/2011 to 12/07/2011.

<b>Legs</b>	<b>Docking places</b>	<b>Docking dates (dd/mm/yyyy)</b>
1	Cadiz (Spain) - Rio de Janeiro (Brazil)	14/12/2010-13/01/2011
2	Rio de Janeiro (Brazil) – Cape Town (South Africa)	17/01/2011-06/02/2011
3	Cape Town (South Africa) – Perth (Australia) – Sydney (Australia)	11/02/2011-13/03/2011-30/03/2011
4	Sydney (Australia) – Auckland (New Zealand) – Honolulu (Hawaii)	04/04/2011-13/04/2011-08/05/2011
5	Honolulu (Hawaii) – Panama (Panama) - Cartagena de Indias (Colombia)	13/05/2011-10/06/2011-13/06/2011
6	Cartagena de Indias (Colombia) – Cartagena (Spain)	19/06/2011-14/07/2011

4

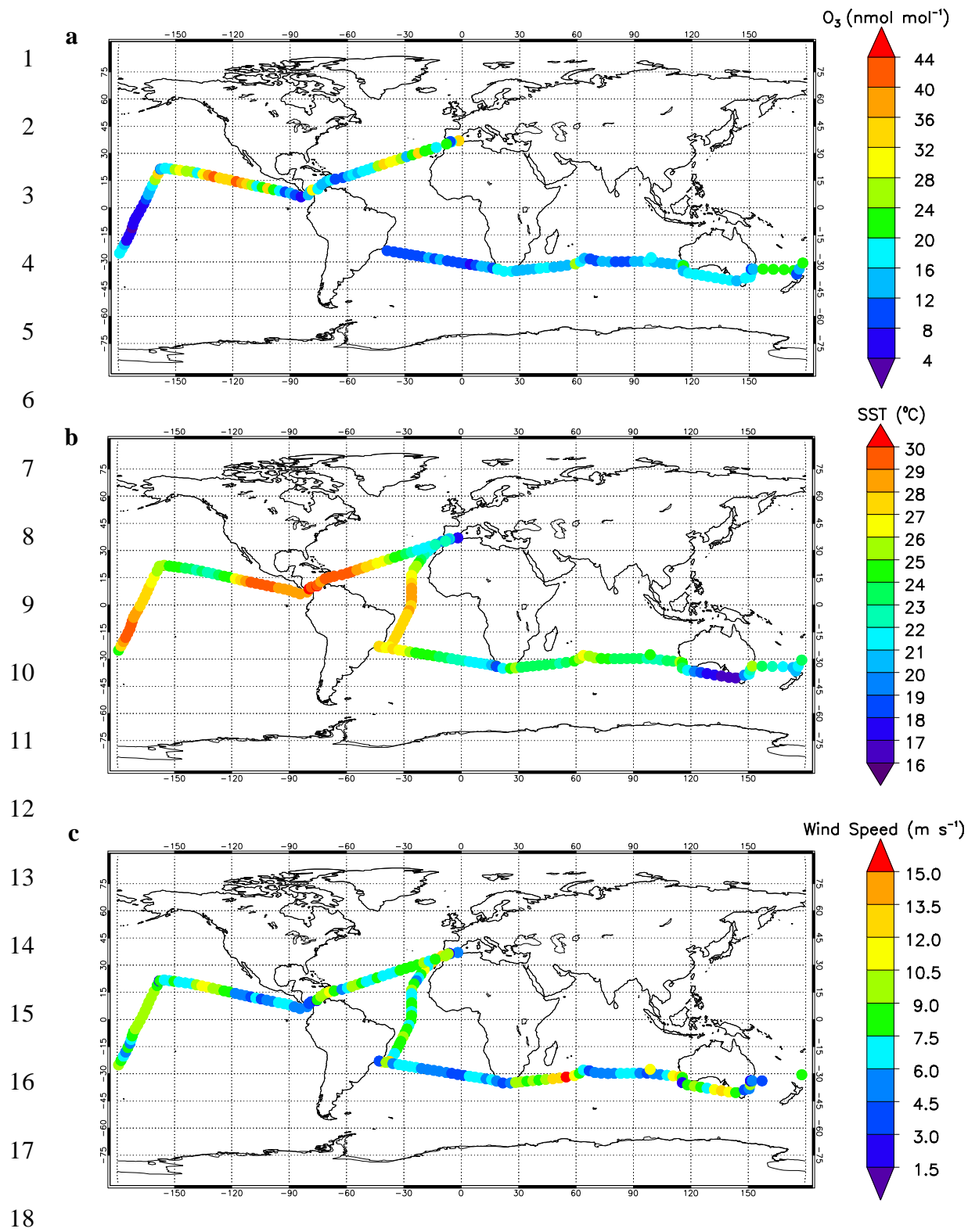
5



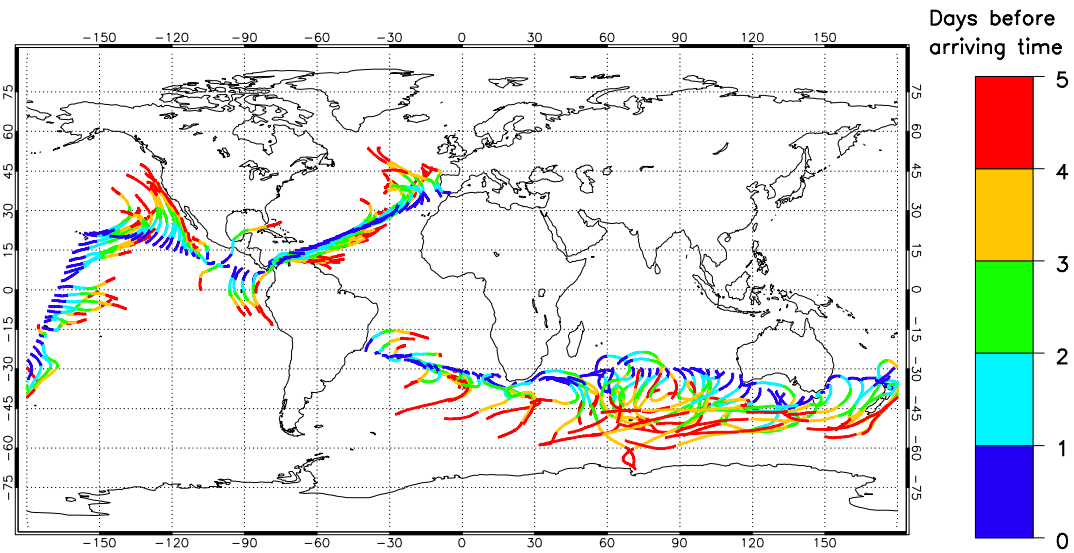
1 Table 2. Summary of the O<sub>3</sub> and ancillary parameters measured during Malaspina 2010. The  
2 data correspond to daytime average values concurrent with the IO measurements gathered  
3 during the expedition (Fig. 1).

<b>Parameter</b>	<b>Mean</b>	<b>Std</b>	<b>Minimum</b>	<b>Maximum</b>
O <sub>3</sub> (nmol mol <sup>-1</sup> )	16.0	9.4	3.4	42.4
ws (m s <sup>-1</sup> )	7.0	2.0	3.3	11.6
SST (K)	298.9	2.9	291.6	303.0

4



19 Figure 1. Observations of surface ozone and ancillary parameters during Malaspina 2010  
 20 (daily average). a. O<sub>3</sub> mixing ratios. b. Sea surface temperature. c. Wind speed. See also Table  
 21 2.  
 22

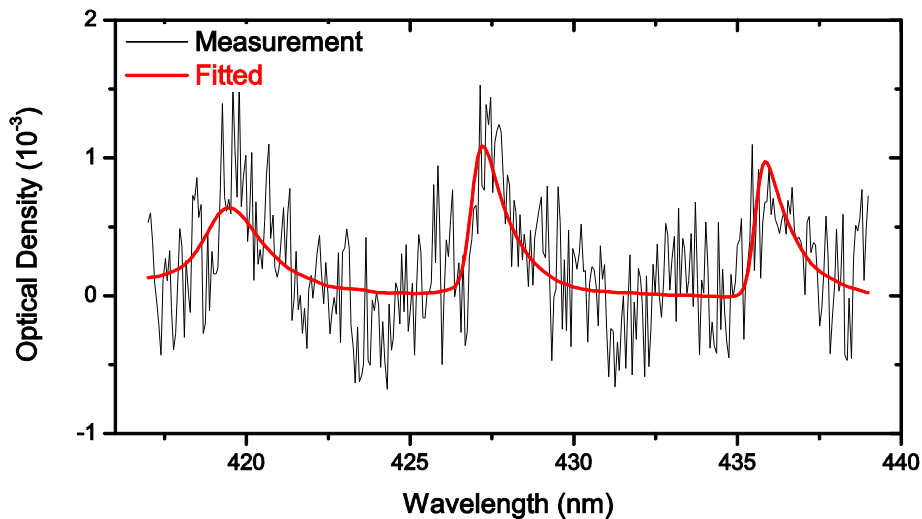


1

2 Figure 2. Backward trajectories of the air masses arriving at noon on every day of the  
 3 Malaspina's cruise. They were calculated using HYbrid Single-Particle Lagrangian Integrated  
 4 Trajectory (HYSPLIT, Draxler and Rolph, 2014).

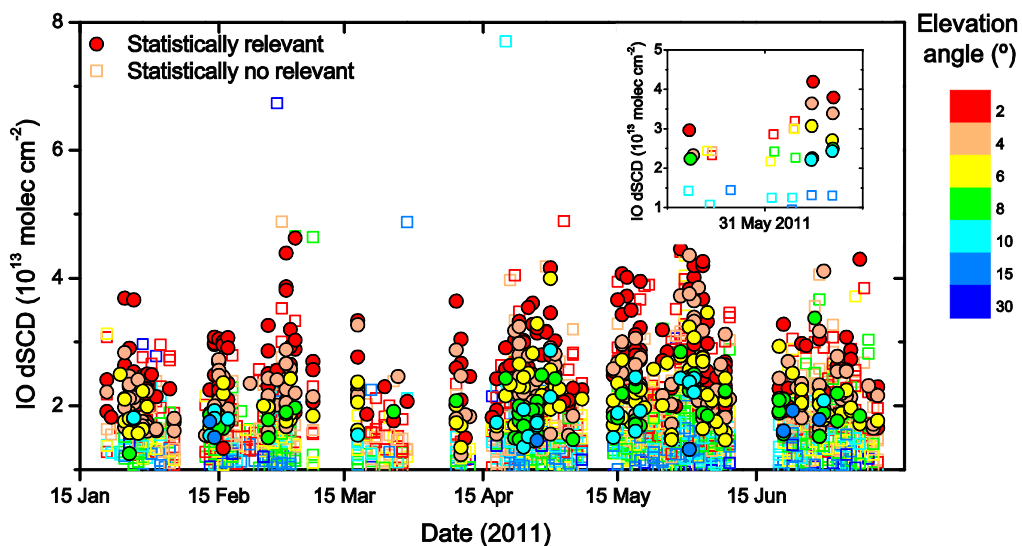
5

a



1

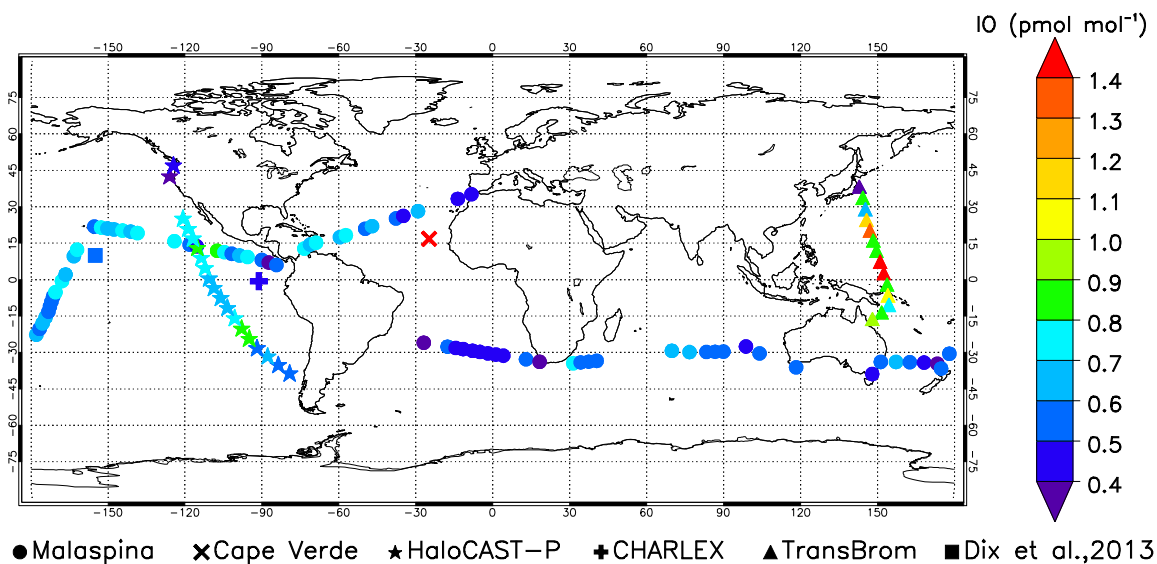
b



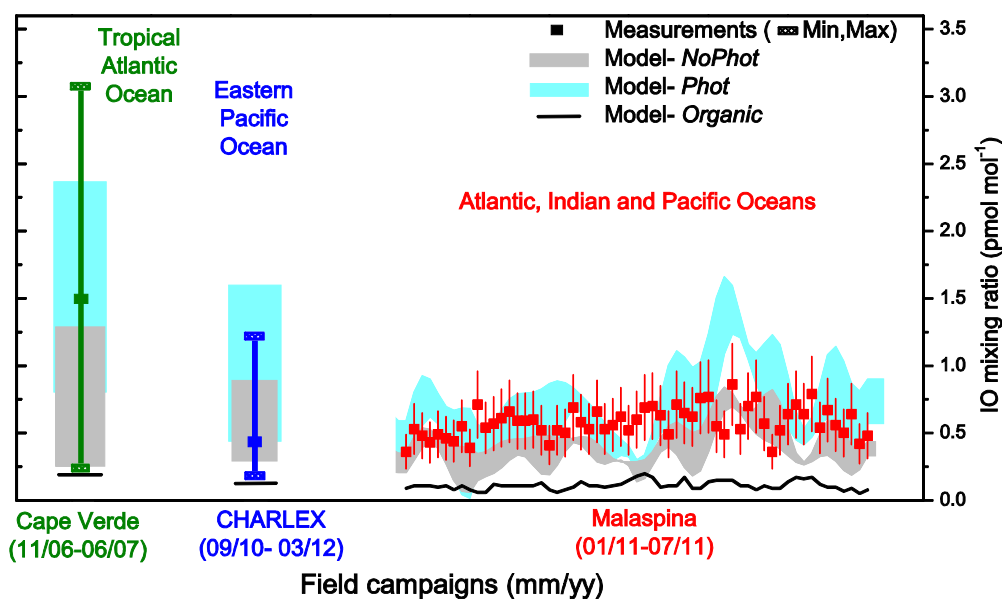
2

3 Figure 3. Retrieval of IO during the Malaspina 2010 circumnavigation. a. Example of a  
 4 typical IO spectral fit during the expedition. The particular spectrum was taken on the 31<sup>st</sup>  
 5 May 2011 (3pm LT, 53° SZA) in the Eastern Pacific for a 2° elevation angle. The black line  
 6 represents the measured IO optical density and the red line the retrieved one after the DOAS  
 7 retrieval. This fit resulted in an IO dSCD of  $(3.8 \pm 0.3) \times 10^{13}$  molecules  $\text{cm}^{-2}$  (i.e., IO vmr of  
 8  $0.8 \pm 0.1$   $\text{pmol mol}^{-1}$ ), with a residual optical density of  $3.9 \times 10^{-4}$  (root mean square). b.  
 9 Timeline of the IO dSCD observed during the expedition. Statistically relevant data (i.e., data  
 10 above the quality filters, SI) are shown with filled circles, and the non relevant data with

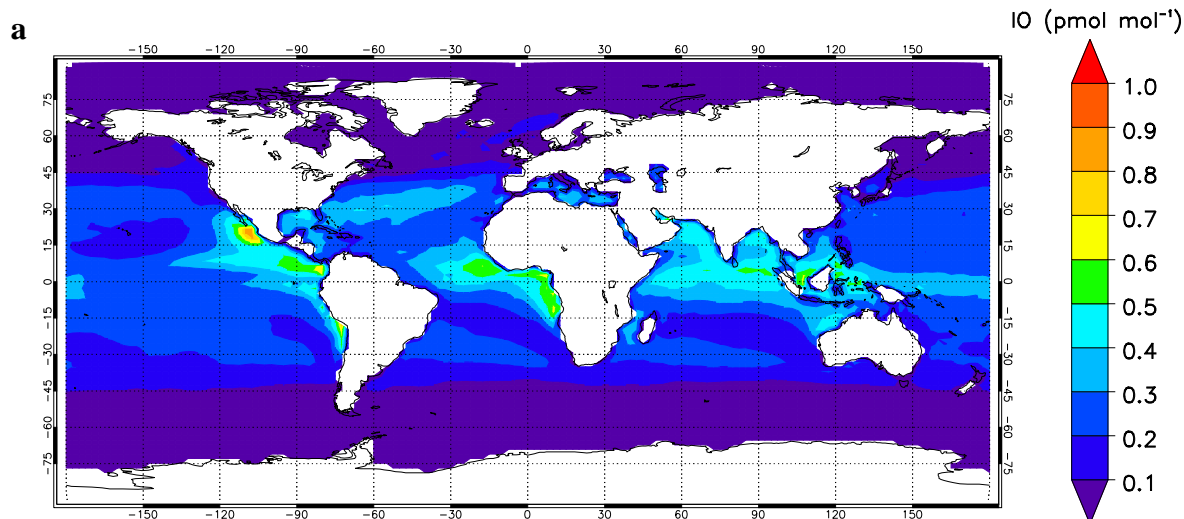
- 1 empty squares. The inset shows the daily evolution of IO dSCD for the 31<sup>st</sup> of May 2011. The
- 2 colour code indicates the elevation angle of the measurements.
- 3



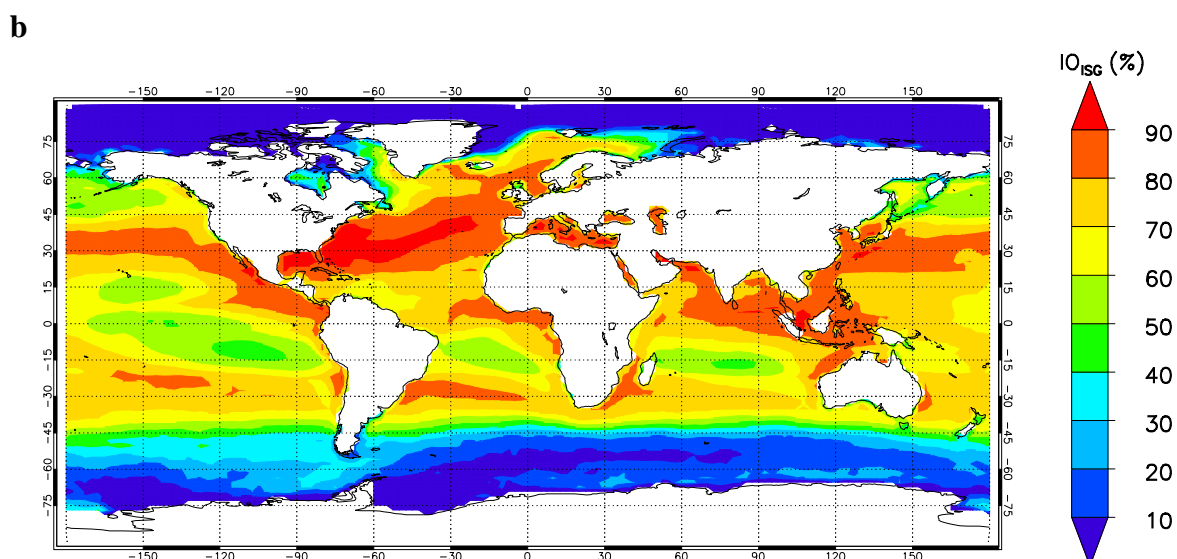
1  
 2 Figure 4. Iodine oxide observations in the global marine boundary layer. IO mixing ratios (in  
 3  $\text{pmol mol}^{-1}$ ) are shown for five different field campaigns (Malaspina (this work), CHARLEX  
 4 (Gómez Martín et al., 2013a), TransBrom (Großmann et al., 2013), HaloCAST-P (Mahajan et  
 5 al., 2012), and Cape Verde (Read et al., 2008; Mahajan et al., 2010); and also for the MBL  
 6 measurements reported by Dix et al (2013) during one research flight. For the three ship  
 7 campaigns (Malaspina, HaloCAST-P and TransBrom) daytime averaged values are shown.  
 8 For the long-term measurements on the Galapagos and the Cape Verde Islands (referred to as  
 9 CHARLEX and Cape Verde, respectively), the mean daytime IO values observed throughout  
 10 the campaigns are given.  
 11



1  
2 Figure 5. Measured and modelled IO mixing ratios in different field campaigns and oceans.  
3 For the two long-term campaigns on islands (Cape Verde- in green- and CHARLEX- in blue)  
4 the mean daytime IO mixing ratio observed during the whole campaign period is given (filled  
5 squares), together with the minimum and maximum observed values (dashed rectangles)  
6 (Read et al., 2008; Mahajan et al., 2010; Jones et al., 2010). In the case of the Malaspina  
7 circumnavigation (in red), daytime averaged IO mixing ratios are provided (filled squares)  
8 along with their error (see also the SI). The shaded areas represent the standard deviation of  
9 the modelled fields for the *NoPhot* (gray) and *Phot* (cyan) *Base* scheme. For comparison  
10 purposes the IO vmr modelled considering only the organic iodine precursors (*Organic* run)  
11 are also included (solid black line).  
12



1  
2

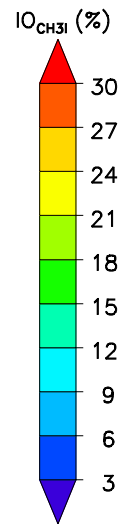
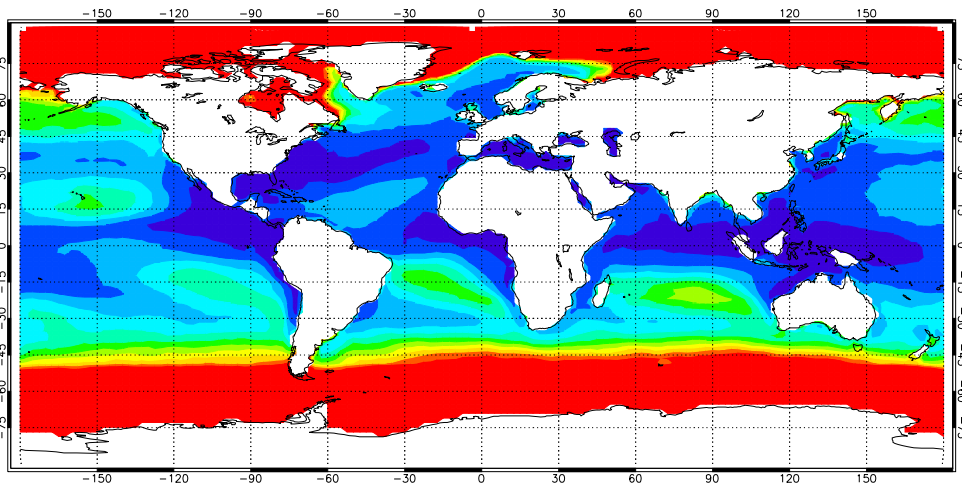


3  
4  
5  
6  
7  
8

Figure 6. Simulated IO in the global marine environment (annually averaged). a. Geographical distribution of the total IO budget in the MBL (i.e.,  $\text{IO}_{\text{ISG}+\text{OSG}}$ ), in units of vmr ( $\text{pmol mol}^{-1}$ ). b. Percentage contribution of the ISG emissions to the budget of IO in the global MBL.

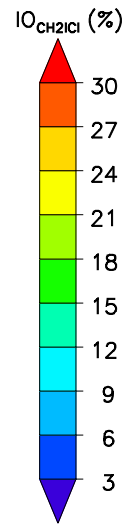
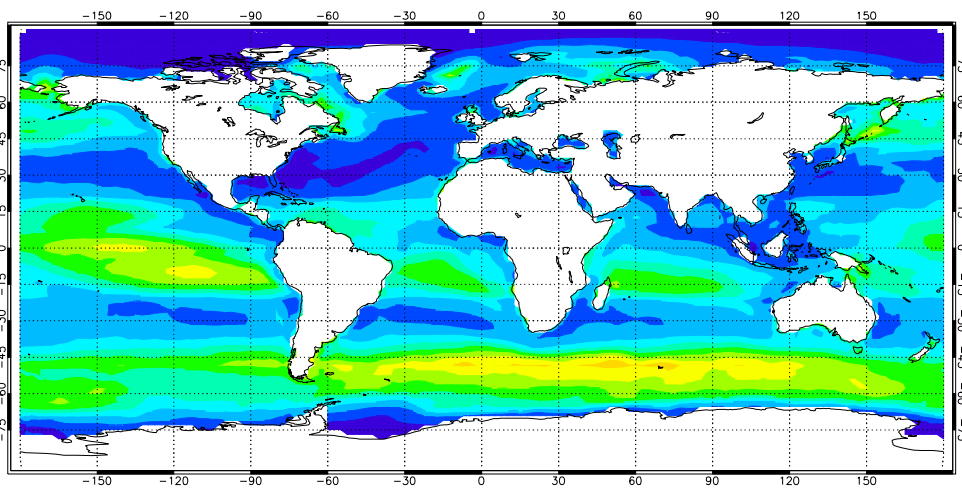


**a**

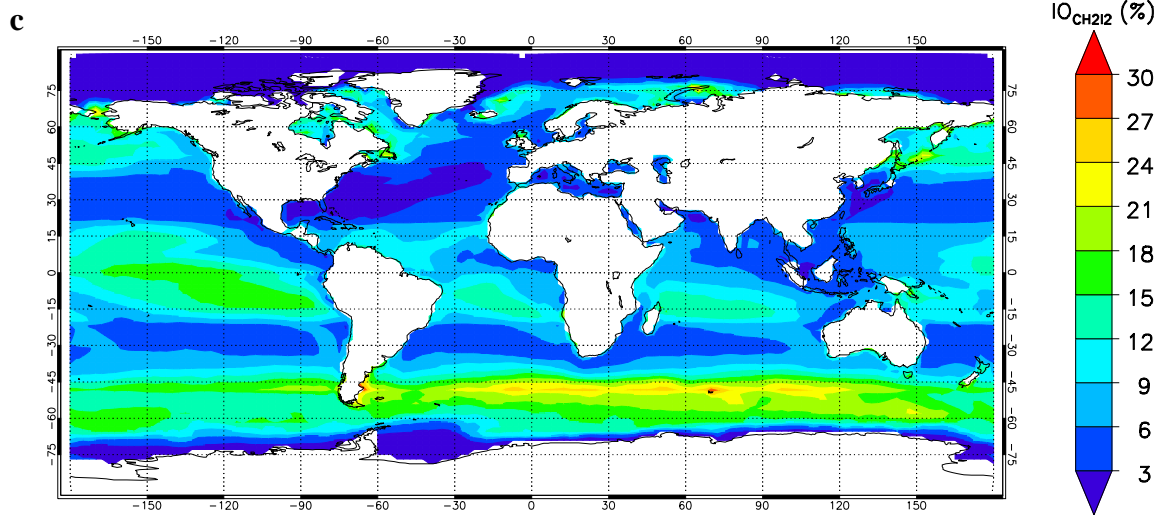


1

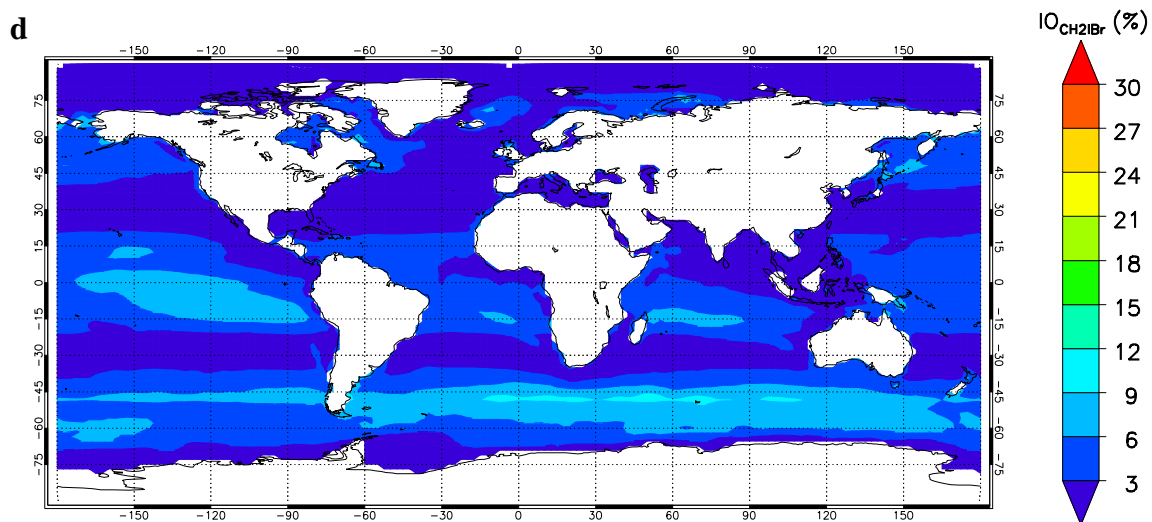
**b**



2



1



2

3 Figure 7. Simulated percentage contribution of the different short-lived iodocarbons (a.  $CH_3I$ .  
 4 b.  $CH_2ICl$ . c.  $CH_2I_2$ . d.  $CH_2IBr$ ) to the IO budget in the marine environment. Note that, for  
 5 comparison purposes, the colour code is the same in the four panels. Also note that these  
 6 model simulations do not include iodine emissions from ice surfaces. For the absolute values  
 7 of the OSG emissions, please refer to the study of Ordóñez et al., 2012.

8